Electronic Supplementary Material (ESI) for Physical Chemistry Chemical Physics.

Thermochemical unification of molecular descriptors to predict radical hydrogen abstraction with low computational cost

Tom M. Nolte, Thomas Nauser, Lorenz Gubler, A. Jan Hendriks, Willie J. G. M. Peijnenburg

SUPPLEMENTARY INFORMATION

CONTENT

S1. Data selection
S2. Descriptor calculation
 Figure S1. Rate constants for reaction with $OH^{\bullet}$ versus E_{LUMO}, E_{HOMO} and E_{HOMO}-E_{LUMO}.
 Figure S2. Rate constants for electron transfer to $OH^{\bullet}$ versus E_{HOMO}, and correction for atomic orbital coefficients c_{HOMO}^{2}
 Table T1. Data used for construction of Figure S2.
 Figure S3. Rate constants for electron transfer and hydrogen abstraction by $OH^{\bullet}$ versus E_{HOMO}
 Figure S4. Rate constants for electron transfer and hydrogen abstraction by $OH^{\bullet}$ versus ΔG_r
 Figure S5. Rate constants for hydrogen abstraction by $OH^{\bullet}$ versus E_{HOMO} (class-specific regressions).
 Figure S6. Thermochemical cycle for H-abstraction
S3. Quantum-chemical corrections
 Figure S7. The offset of the LFERs for reactions involving $OH^{\bullet}$ versus the local dipole moment
 Figure S8. Parametrization of the Eyring equation using rate constants log (k_r) for reaction with $OH^{\bullet}$ and the selected parameters
 Table T2. Parameters used to develop the model for k_r ($OH^{\bullet}$)
S4. Model validation
 Figure S9. Evaluation of Eq. 8 via selectivity.
 Figure S10. Parameter sensitivity analysis.
 Table T3. Parameters used to predict k_r ($H^{\bullet}$)
 Figure S11. Prediction of k_r ($H^{\bullet}$)
 Table T4. Parameters used to predict k_r ($CH_3^{\bullet}$)
 Figure S12. Prediction of k_r ($CH_3^{\bullet}$)
S5. Radical electrophilicity
 Figure S13. Radical electrophillicity versus E_{SOMO}
 Table T5. Radical electrophilicity and E_{SOMO} values
S6. Radical addition
 Figure S14. The rate constant for addition of $OH^{\bullet}$ versus E_{HOMO}
S7. Discussion of associated uncertainties

S1. Data selection

Data for the bimolecular reaction rate constants (k_r) in water was gathered from the open literature. We chose kinetics data for ET as well as HA by the radical $OH^\bullet$ as frame of reference, whereas we validated using data for $OOH^\bullet$, $H^\bullet$ and $CH_3^\bullet$. Notable sources were the studies by Luo et al. [1], the Buxton et al. [2] and Dorfman and Adams [3] reviews and the NDRL/NIST Solution Kinetics Database [4], in which data were categorized based on endpoint, method, similarity of values, etc., allowing comparison and quality selection. The compounds include a broad range of chemical functionalities, e.g. double bonds, inorganic and aliphatic substructures. Metal (organic) complexes and inorganic molecules were added to broaden the applicability domain. The total dataset contained approximately 500 chemicals with aqueous-phase rate constants (upon request), determined via various methods including laser flash photolysis and pulse radiolysis (X, γ, and e-) techniques.

S2. Descriptor calculation

Structures were pre-optimized using OpenBabel [5] via SMILES (Simplified Molecular Input Line Entry System) input. Molecular Orbital (MO) calculations were carried out using the semi-empirical Hamiltonian Parameterization Method 7 (PM7) with 92 geometrical segments (NSPA), within the program package MOPAC Version 2016 [6]. Semi-empirical MO theory was chosen to limit the computational time required, but we increased the criteria for terminating electronic and geometric optimizations by a factor 100 to acquire more precise results. *Ab initio* or other computationally intensive methods were deemed not useful for our purpose due to the size of the dataset and molecules. The PM7 method was chosen because of a recent correction in the derivation of interaction energies via incorporation of van der Waals attraction and hydrogen bonding [7], yielding satisfactory results in previous studies [8, 9]. The quantum-chemical calculations for $OH^{\bullet}$, $OOH^{\bullet}$, $H^{\bullet}$ and $CH_3^{\bullet}$ were performed using the same (semi-empirical) parameterization [6, 7]. Hence, we benefit from thermochemical additivity and comparison is straightforward. The water solvent (ε = 78.4) was described using the COSMO (Conductor-like Screening Model) approximation. The accuracy of MOPAC's 3D structure generation is evaluated elsewhere: relevant information, e.g. heat of formations, can be accessed here: http://openmopac.net/PM7_accuracy/Heats_of_Formation.html

For HA on non-symmetric molecules, E_{HOMO} values were calculated upon removing the proton from the most substituted, electron-rich, and conjugated position, and R–H group with the lowest pK_a (e.g. in α-position to an electron donating functional group). The energy of the sigma electrons of the deprotonated R-H bond is envisioned as being a proxy of the transition state of HA (Fig. S6). A typical calculation took approximately 5 s on a standard desktop computer.

The electronic structure of the reaction partners and energies of the frontier orbitals and interaction between them can be significantly altered by (de-)protonation, *i.e.* pK_a and pH. As a result, the reaction kinetics are affected as was previously shown for related oxidants [8, 9]. Thus, pH-corrected ionic speciation states were implemented for the QC calculations. Therefore, ion speciation states at experimental pH were determined using pK_a/pK_b [10]. pK_a values were both taken from the literature (T2-T4) and calculated via atomic charges and site-specific regression using ChemAxon[11]. The accuracy of this method is detailed elsewhere [12, 13].

If the rate constant was measured at pK_a~pH, descriptors (E_{HOMO}, E_{LUMO}, orbital coefficients, dipole moment, Fukui delocalizabilities, etc.) were calculated for both speciation states [8, 9] and averaged. Note that protonation cannot explain the offsets and difference slopes (σ_{LFER}) between the LFERs: the differences in slopes (σ_{LFER}) and between different H-donors remained after (de)protonation.

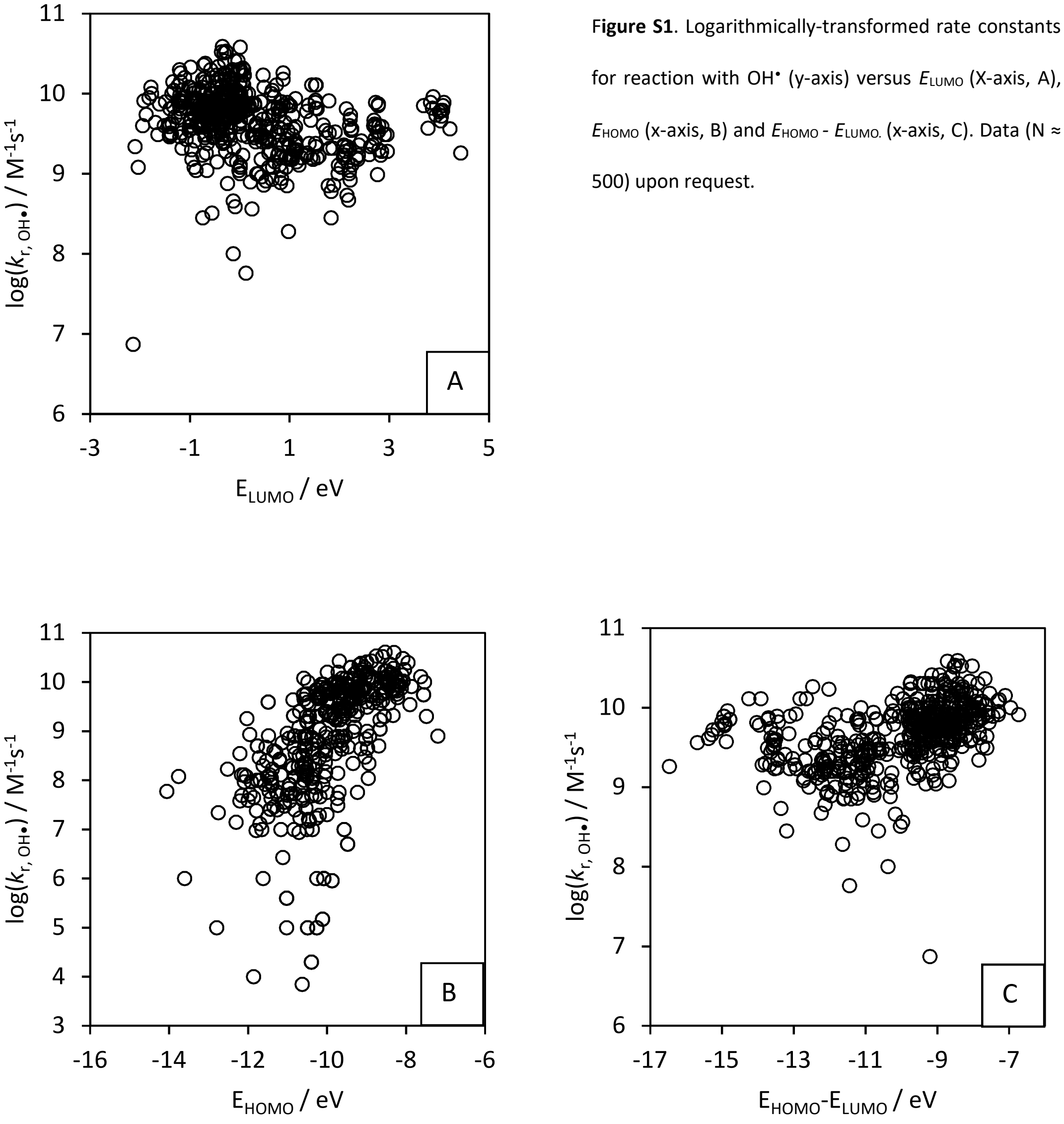

Figure S1. Logarithmically-transformed rate constants for reaction with $OH^•$ (y-axis) versus E_{LUMO} (X-axis, A), E_{HOMO} (x-axis, B) and E_{HOMO} - $E_{LUMO.}$ (x-axis, C). Data (N ≈ 500) upon request.

When we take into account only the term $\Delta G_{\mathrm{ET,ox}}$, ~95% of the ET and HA rate constants (N ≈ 500, reacting with the $OH^•$ radical) were within 2 orders of magnitude of the expected value (Fig. S1B; S3B, $p < 1x10^{-5}$). As expected [14, 15], the correlation with E_{LUMO} was lower (Fig. S1A) than with E_{HOMO}. The correlation with E_{HOMO} found by Minakata [16] for $OH^•$ was slightly higher. Our data, however, cover substrates with a much broader range of structural elements.

S2-1. Electron transfer

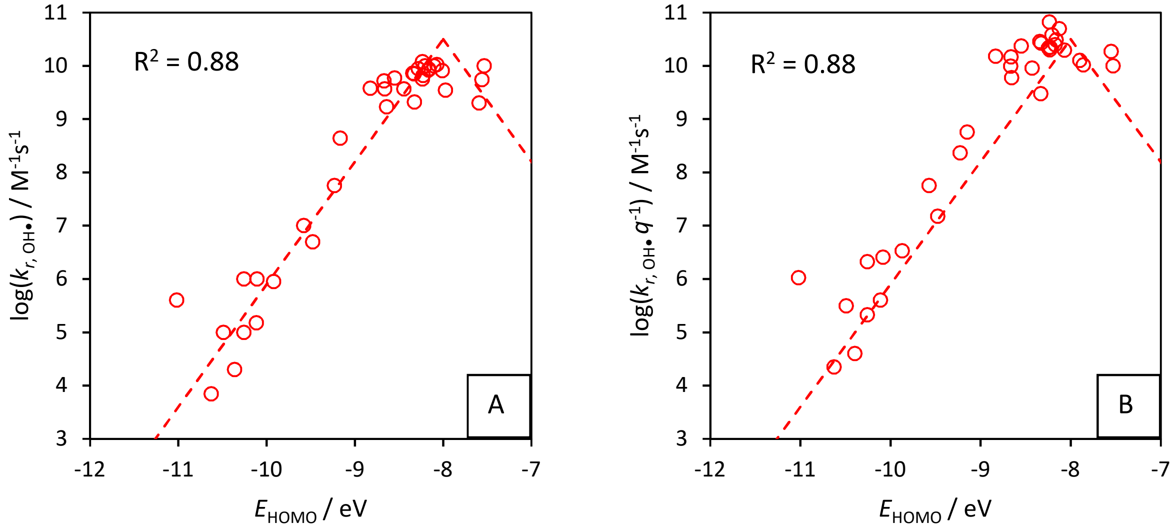

Figure S2. Logarithmically-transformed rate constants for electron transfer to OH$^{\bullet}$ (y-axis) versus E_{HOMO} (X-axis, A). B denotes the rate constants corrected for q, via atomic orbital coefficients (c_{HOMO}^{2}). Dashed lines denote theoretical ranges.

Table T1. Data used for construction of Figure S2.

Compound name	E_{HOMO}	c_{HOMO}^2	k_r(exp)	Refs
dihydrogenphosphate ion	-10.36	0.50	2.0E04	[2]
peroxodisulfate ion	-10.26	0.47	1.0E05	[2]
hydrogenphosphate	-10.12	0.37	1.5E05	[2]
phosphate ion	-10.11	0.39	1.0E06	[2]
Pyrophosphate ion	-9.92	0.27	9.0E05	[2]
bromate ion	-9.48	0.33	5.0E06	[2]
nitrilotriacetatocobaltate(III)	-9.17	0.77	4.4E08	[2]
selenate ion	-8.83	0.25	3.8E09	[2]
Di(tert-butyl)sulfoxide	-8.67	0.53	5.2E09	[1]
2,4-dichlorophenol	-8.33	0.27	7.1E09	[1]
peroxomonosulfate ion	-8.33	0.70	2.1E09	[2]
Sulfisoxazole	-8.23	0.30	6.6E09	[1]
3,4-Dihydroxyacetophenone	-8.21	0.26	1.0E10	[1]
N,N,N',N'-tetramethyl-p-phenylenediamine	-8.11	0.20	1.0E10	[1]
ferrocyanide ion	-8.07	0.53	1.1E10	[2]
Selenodicysteine	-8.01	0.78	8.1E09	[1]
5,7,7,12,14,14-hexamethyl-1,4,8,11-tetraazacyclotetradecanenickel(II) ion	-8.64	0.28	1.7E09	[2]
sulfite ion	-7.56	0.30	5.5E09	[2]
Pentabromophenoxide	-8.55	0.25	5.9E09	[4]
Pentachlorophenoxide	-8.66	0.25	3.7E09	[4]
Promazine	-8.45	0.41	3.7E09	[4]
Chlorpromazine	-8.28	0.41	8.8E09	[4]
1-Aminonaphthalene-4-sulfonate	-8.34	0.26	7.3E09	[4]
Methylene Blue	-8.24	0.18	1.2E10	[4]
peroxodisulfate ion	-10.26	0.47	1.0E06	[2]
technetate(IV) ion	-7.59	0.86	2.0E09	[2]
Metiazinic acid	-8.17	0.34	8.4E09	[4]
$Ni(CN)_4^{2-}$	-7.54	1.00	1.0E10	[4]
4-Fluorophenoxide	-8.16	0.28	8.7E09	[4]
4-Bromophenoxide ion	-8.23	0.28	5.7E09	[4]
Myoinositol sulfate	-9.58	0.18	1.0E07	[4]
ClO_3^-	-11.02	0.38	4.0E05	[4]
selenite ion	-7.98	0.27	3.5E09	[2]
Tetrahydroxyborate	-10.49	0.32	1.0E05*	[4]
Oxomalonate	-9.23	0.25	5.7E07	[4]
PFOA	-10.63	0.31	7.0E03	[17]

* reported as <1E6, taken as 1E5

Figure S2 (and Table T1) illustrate a validation of the relevancy of E_{HOMO} values. In contrast to HA, for ET only an electron transfers. Marcus theory characterizes the TS energy for ET (assuming no electronic coupling) as:

Eq. S0-1 $$\Delta G_{ET}^{\ddagger} \approx \frac{(\Delta G_{ET}+\lambda)^2}{4\lambda}$$

Herein, ΔG_{ET} is the reaction driving force, and λ the reorganization energy of reactants and solvent during the transition state. By differentiation of Eq. S0-1, we get:

Eq. S0-2 $$\Delta(\Delta G_{ET}^{\ddagger}) = \left[\frac{(\Delta G_{ET}+\lambda)}{2\lambda}\right]\Delta(\Delta G_{ET})$$

Thus, we can describe the LFER substituent constant σ_{LFER} for ET as:

Eq. S0-3 $$\sigma_{LFER} = \frac{(\Delta G_{ET}+\lambda)}{2\lambda}$$

The derivations are similar for S_N2 reactions [18, 19]. Thus, σ_{LFER} is intrinsically connected to λ.

The LFER results for ET in the current study (Fig. S2) show a uniform value for σ_{LFER}. This indicates 'little' variation in λ. Seeing as $\Delta G_{\mathrm{TS}}^{\ddagger}$ also can also involve solvent reorganization, it also indicates little variation in $\Delta G_{\mathrm{TS}}^{\ddagger}$. For mechanistically similar reactions, e.g. outer-sphere ET, λ (and $\Delta G_{\mathrm{TS}}^{\ddagger}$) might be a constant factor. Thus, S0-1 can be interpreted such that ΔG_{ET} represents the initial perturbation of the system as it begins to move along the reaction coordinate [20]. In other words, comparison of ΔG_{ET} gives also $\Delta G_{ET}^{\ddagger}$ (i.e. $\Delta G_{ET}^{\ddagger} \propto \Delta G_{ET}$).

The σ_{LFER} values for ET did not statistically differ from those for HA (2SD). However, the root-mean squared error of the LFER for ET was lower than that for HA (Fig. S4B), and no 'families of compounds' were observed (as in Fig. 6B). This shows that either reorganization energies λ are smaller for ET as compared to HA, or the difference is the result of an electronic coupling, or both factors apply.

S2-2. Proton transfer

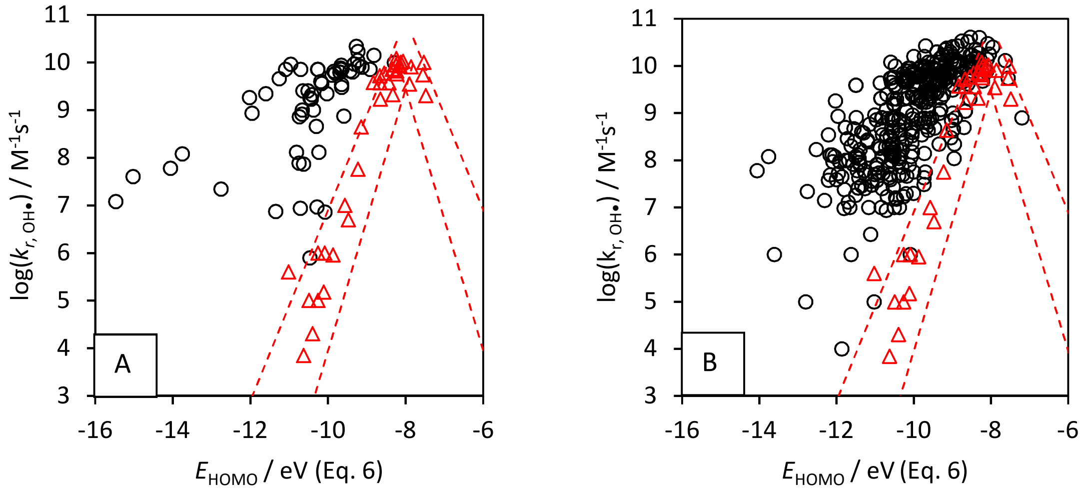

Figure S3. Logarithmically-transformed rate constants for electron transfer by $\mathrm{OH}^{\bullet}$ (y-axis) versus E_{HOMO} (x-axis), red triangles. Hydrogen abstraction reactions are also shown (black circles). Figure S3A denotes compounds with experimental pK_a whereas S3B denotes all compounds, including those with estimated pK_a. Dashed lines indicate the theoretical ranges for electron transfer, drawn using 2.0 and 2.7 p(k_r)/eV, and correspond to E_{SOMO} ($\mathrm{OH}^{\bullet}$) = 8.0(±0.2) eV.

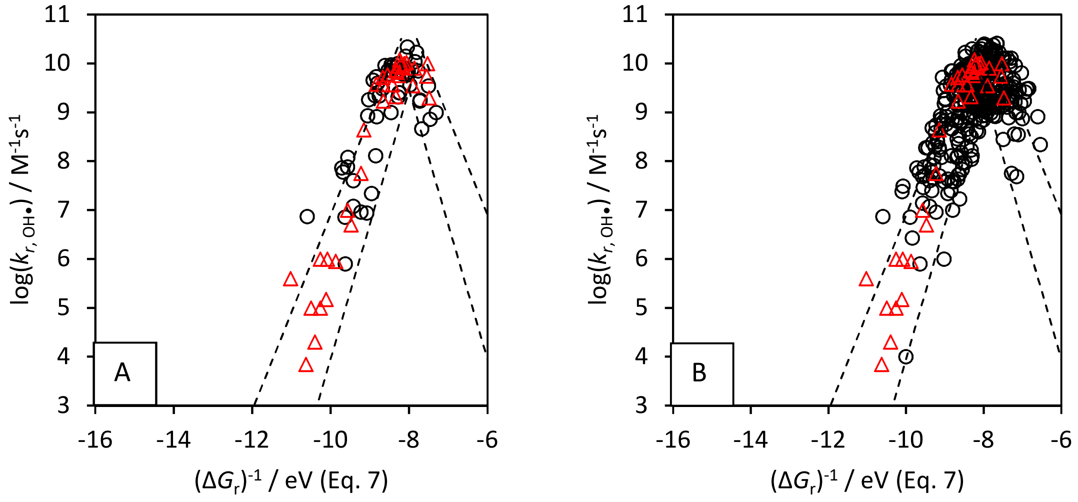

Figure S4. Logarithmically-transformed rate constants for the reaction of $\mathrm{OH}^{\bullet}$. A and B involve the same compounds as in Fig. S3A and B (resp.), but the data are plotted versus the outcome of calculations using Eq. 6. Figure S4A denotes compounds with experimental pK_a whereas S4B denotes all compounds with predicted pK_a [11]. Black circles denote hydrogen abstraction. For the sake of completeness, electron transfer reactions are also shown (red triangles). Dashed lines indicate the theoretical ranges based on ET.

The energy levels of the HOMO and SOMO orbitals often differ. Therefore, the stabilization as a result of their overlap (Eq. 5) is limited and ET from the HOMO is highly energy consuming. For this reason, (oxidative) one-electron transfer is a rather slow reaction pathway for $OH^\bullet$ as well as for $OOH^\bullet$, $H^\bullet$ and $CH_3^\bullet$ [2]. In other words, if rate determining, lowest reaction rates are observed *via* this pathway. E_{HOMO} defines the lower-limit of the linear free-energy relationship (LFER), with σ_{LFER} (±2SD) is 2.2±0.2 p(k_r)/eV.

Fig. S3B shows the correlation of log k_r with the free energy of reaction, according to equation (6). This plot ignores the statistical factor *q*, equation (1), and influences on the transition state, Fig. 2 and equation (3). A portion of the scatter in LFERs for HA ($\Delta(\Delta G)$) involving non-symmetric molecules (N ≈ 500, Fig. S4B) can be explained by the presence of multiple H atoms, and/or erroneously assigned abstraction sites. The expected values for k_r of these compounds referred to single R–H bonds only.

E_{HOMO} relates to HA rates as well, albeit slopes for LFERs involving different H-donor types differ: 0.6-0.7 p(k_r)/eV for alkanes (Fig. S5, S3A; [21]), 0.9(±0.2) for hydrofluorocarbons and ethers [22] and 1.1 for alcohols [21] and arenes [23]. Also, 1.6-2.1 p(k_r)/eV for aliphatic amines are reported (Fig. S5). The slopes of the regressions with E_{HOMO} for HA (0.6-2.2 p(k_r)/eV) differ from those found for ET (2.2±0.1 p(k_r)/eV, Fig. S3A). Clearly, the large scatter in Fig. S3A (k_r versus E_{HOMO}) indicates the presence of driving forces other than electron transfer (Eq. 6). This illustrates that E_{HOMO} is insufficient to describe HA [9, 24].

The differences in slopes (and offsets) in the regressions for HA with E_{HOMO} clearly arise from differences in pK_a between compounds. Similarly, linear inverse relationships between pK_a and $E_{ox}(A^-)$ are often observed [25], with slopes near unity, which is because of a balancing of destabilizing and stabilizing substituent effects.

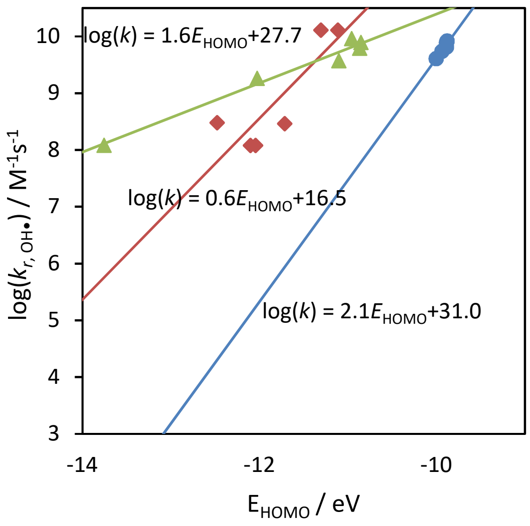

Figure S5. Logarithmically-transformed rate constants for hydrogen abstraction to OH$^\bullet$ (y-axis) versus E_{HOMO} (X-axis, A). Green triangles: alkanes, Red diamonds: protonated aliphatic amines, Blue circles: deprotonated aliphatic amines. Solid lines denote data fits.

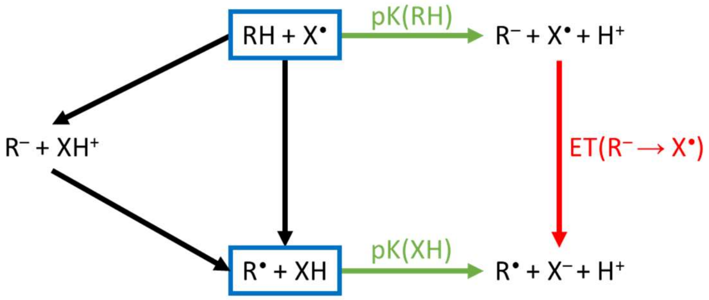

Figure. S6. Thermochemical cycle for H-abstraction. The reaction driving force for both sequential (left) or concerted (center) mechanisms is described using proton transfer (pK_a, green arrows) and electron transfer (red arrow). Electron transfer in absence of protolysis (black). pK_a characterizes a charge-transfer interaction and are related to the partial charges Q on R–H (the positive charge Q_H on H). E.g. for congeneric molecules, a universal factor of acidity can be calculated, e.g. via [26] $pK_a(R-H) = 49.04 - 134.6Q_H$.

S2-3. Calculation of ΔG_r

The detailed version of Equation 4 in the main document is given by [27]:

Eq. S1
$$\Delta G_r = \underbrace{\frac{2\left(\beta c_{SOMO,X^\bullet}\, c_{HOMO,R^-}\right)^2}{E_{SOMO,X^\bullet} - E_{HOMO,R^-}}}_{\Delta G_{ox}} - \underbrace{\frac{Q_{X^\bullet}\, Q_{R^-}}{\varepsilon\, r}}_{\Delta G_{charge\ tr.}}$$

In Equation S1, $E_{SOMO,X^\bullet}$, E_{HOMO,R^-} and E_{LUMO,R^-} are the energies of the frontier orbitals of the two reactants: the radical ($X^\bullet$) and the closed shell molecule (R^-). $c_{SOMO,X^\bullet}$ is the effective atomic orbital coefficient (scalar) of the SOMO, and c_{HOMO,R^-} and c_{LUMO,R^-} are the effective atomic orbital coefficients of the HOMO and LUMO, respectively.

The reductive term in Eq. S1 can be neglected for oxidations, *i.e* if the probability for the electron being transferred from the SOMO to the LUMO is tiny compared to it being transferred from the HOMO to the SOMO (i.e. E_{SOMO}-E_{HOMO} <<< E_{LUMO}-E_{SOMO}). In Fig. S3, we plotted E_{HOMO} according to equation (5) against experimental data (N ≈ 500) of log k_r. Panel A thereof illustrates that E_{HOMO} (pure electron transfer, red triangles) reflects the lower limit of the rate constant (Fig. S3A).

The third (coulombic) term is a correction for charge-transfer during the transition state, which is influenced by the reagent charges *Q*, their distance *r* and permittivity ε of the medium. β is the resonance integral for the interaction between the orbitals and refers to orbital geometries and the 'effectiveness' of their overlap. The formula was developed to include charge transfer in general, but in the current study it is adapted for the transfer of protons (positive charge).

The term $2\left(\beta c_{SOMO,X^\cdot}\, c_{HOMO,R^-}\right)^2$ denotes a contribution from shape and spatial density, and can be considered constant when the HOMO electrons in 'similar' molecules are equally distributed. The terms β and $c_{SOMO,X^\bullet}$ can be combined into α, which denotes a contribution from both shape and spatial density. α can be considered a constant factor:

Eq. S2
$$\Delta G_r = \alpha \frac{c_{HOMO,R^-}^{2}}{E_{SOMO,X^\bullet} - E_{HOMO,R^-}} - \frac{Q_{X^\bullet} Q_{R^-}}{\varepsilon r}$$

With inclusion of the statistical factor q, we still found three “families” of datapoints with different offsets for the regressions. (Fig. 6B and S8D).

S3. Quantum-chemical corrections

Following LFER regressions, calculations were refined (see Eq. 7 and 8) for symmetric molecules using transition-state (TS) theory via empirical selection of the molecular properties influencing TS energies. Stepwise regression was used to determine the relevance of descriptors.

The HOMO-LUMO energy gap (Fig. S1C) is easily retrievable and is often used to characterize $\Delta G^{\ddagger}$ [14, 28-30]. E_{HOMO}-E_{LUMO} may even correlate with antioxidant activity [31, 32]. The correlation between k_r ($OH^{\bullet}$) and E_{HOMO}-E_{LUMO} was low ($N \approx 500$, $R^2 \approx 0.1$, $p < 1 \times 10^{-4}$, Fig. S1C). In `complex` chemicals, the HOMO and LUMO can be part of different functional groups or substructures. More detailed corrections using TS theory are usually needed [33, 34], in our case to characterize the offsets of LFERs.

Rather than E_{HOMO}-E_{LUMO}, were preferred atom-specific indices to characterize $\Delta(\Delta G_{\mathrm{TS}}{}^{\ddagger})$. We distinguished between R–H bond type (either π or σ) via Fukui delocalizability indices (Table T2). Then, the offset between the LFERs (for σ-type and μ-type H donor molecules) were rendered smaller (≈20 kJ/mol, Fig. S8E compared to Fig. S8D). In comparison, the difference in *BDE*s between non-allylic sp^3 C–H bonds (σ) and allylic sp^3 C–H bonds (π) is ≈40 kJ/mol (BDEs ≈445, ≈400 and ≈360 kJ/mol for sp^2 C–H bonds, non-allylic sp^3 C–H bonds, and allylic sp^3 C–H bonds, resp.) [35].

Delocalizability alone was insufficient to fully characterize the offsets between the LFERs. The remaining differences in terms of $\sigma\Delta G^{\ddagger}$ are ≈30 and ≈100 kJ/mol for non-polar compounds compared to polar and zwitterionic compounds, respectively. When the empirical correction based on the dipole moment was included as well (Fig. 5; Eq. 8), the offsets fully disappeared (Fig. S8F compared to S8E). The offsets in Fig. 6B are the result of specific TS effects $\Delta(\Delta G^{\ddagger}_{\mathrm{TS}})$ (see Fig. 2) captured in Fig. 5. Selection of E_{HOMO}, pK_a, delocalizability, dipole moment and empirical fitting (z) using Equation S3 (Eyring-like) resulted in Equation S4.

Equation S3. $$e^{-\Delta G^{\ddagger}} \propto k_r = c_{\mathrm{HOMO}}{}^{2}\left(\sum_{\sigma=1}^{\sigma}\left[e^{(E_{\mathrm{HOMO},\sigma}-b_{\sigma})+e_x} + z_{\sigma}\right] + \sum_{\pi=1}^{\pi}\left[e^{(E_{\mathrm{HOMO},\pi}-b_{\pi})+e_x} - z_{\pi}\mu\right]\right)$$

With $\mathrm{p}K_{\mathrm{a}}(R-H)$ and $\mathrm{p}K_{\mathrm{a}}(X-H)$ being the proton dissociation constants of R–H and the conjugate hydrogen donor X–H of the attacking radical X$^{\bullet}$, respectively, see Fig. S6.

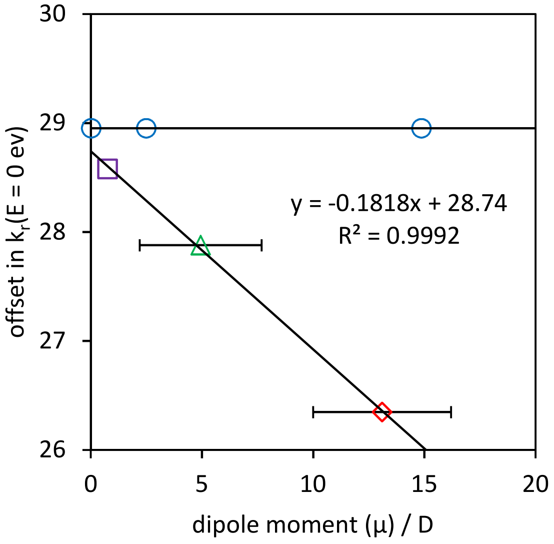

Fig. S7. The offset of the LFERs for reaction with OH$^{\bullet}$ (offset ∝ 1/-Δ*G*‡) plotted versus the local dipole moment at the hydrogen atom. Blue circles denote σ-type H atoms, whereas other symbols denote μ-type H-atoms. Hence, for μ-type hydrogens the local polarity plays a role whereas for σ-type hydrogens it does not.

Eq. S4 $$k_r = c_{\mathrm{HOMO}}{}^{2}\left(\sum_{\sigma=1}^{\sigma}\left[e^{(E_{HOMO,\sigma}-b_{\sigma})+e_x} - 0.51\right] + c\sum_{\pi=1}^{\pi}\left[e^{(E_{\mathrm{HOMO},\pi}-b_{\pi})+e_x} - 0.18\mu_{\pi}\right]\right)$$

With *b* = $2.3RT[\mathrm{p}K_a(RH) - \mathrm{p}K_a(XH)]$. 28.7 was obtained for the offset *c* (electrophillicity of X$^{\bullet}$, taken for OH·), whereas 0.51 and 0.18 were determined empirically for the influence of the dipole moment μ_{π} of R-H on k_r (Fig. S7).

We evaluated the statistical reproducibility of our method: the correlation coefficient (R^2), the squared error (RMSE), and probability values (p) were calculated as indicators of the goodness of fit and correspondence of the relationship between descriptors and log(k_r), respectively.

Table T2. Data used to develop the model Eq. 8 for k_r (OH•) in Fig. S8B-S8F. pK_a for alpha C-H of amino acid analogs were taken to be 16.5, see Stroud et al. (1983).

Compound name	$D_n(r)$	σ	π	E_{HOMO}	pK_a	$c_{\mathrm{HOMO}}{}^2$	μ_π	k_r(exp)	k_r(pred)	Refs
methane	-0.33	4	0	-6.96	55	1.0	-	1.2E8	8.4E7	[4, 11, 36, 37]
octane	-0.43	18	0	-5.66	61	0.7	-	9.1E9	8.4E9	[4, 11, 36, 37]
ethane	-0.38	6	0	-6.42	56	0.9	-	1.8E9	1.8E9	[4, 11, 36, 37]
acetonitrile	-0.53	0	3	-8.13	25	0.5	4.9	2.2E7	3.2E7	[4]
cyanamide	-0.62	0	2	-9.14	10.3	0.4	4.9	8.7E6	8.2E6	[4, 38]
hydrogen	n/a	2	0	-7.94	36	1.0	-	4.0E7	8.8E7	[4, 11]
ammonia	-0.25	3	0	-8.09	36	1.0	-	7.7E7	6.2E7	[4]
acetic acid	-0.59	0	3	-8.63	21.5	0.5	4.9	9.2E6	8.0E6	[4, 11]
acetone	-0.59	0	6	-8.38	19.3	0.5	4.9	1.3E8	1.1E8	[4, 39]
urea	-0.64	0	4	-9.40	15.7	0.4	4.9	7.9E5	8.0E5	[4, 11]
cyclopentane	-0.42	10	0	-5.88	60	0.8	-	3.7E9	2.7E9	[4, 11, 36, 37]
cyclohexane	-0.43	12	0	-5.74	60	0.7	-	6.2E9	6.7E9	[4, 11, 36, 37]
cycloheptane	-0.43	14	0	-5.65	61	0.7	-	7.8E9	9.0E9	[4, 11, 36, 37]
alanine, zwitterion	-0.60	0	1	-7.68	16.5	0.5	13.1	8.3E7	6.7E7	[4, 40, 41]

glycine, zwitterion	-0.60	0	2	-8.22	16.5	0.6	13.1	1.2E7	8.9E6	[4, 40, 41]
aspartic acid	-0.67	0	2	-7.77	16.5	0.6	13.1	3.9E7	7.0E7	[2, 40]
glycine anhydride	-0.64	0	4	-7.69	19.7	0.3	4.9	1.2E9	1.3E9	[4, 11]
glycolamide	-0.60	0	2	-7.60	20.3	0.3	4.9	1.1E9	1.0E9	[4, 11]
sarcosine anhydride	-0.64	0	4	-7.55	19.4	0.2	4.9	2.6E9	2.5E9	[1, 11]
beta-alanine, zwitterion	-0.59	0	2	-7.79	16.5	0.6	13.1	1.1E8	8.0E7	[2, 40]
taurine	-0.47	0	2	-8.15	16.5	0.7	13.1	9.5E6	1.4E7	[4, 40]
n,n-dimethylglycine, zwitterion	-0.57	0	2	-8.14	16.5	0.6	13.1	1.5E7	1.3E7	[40, 41]
tetramethylammonium	-0.35	12	0	-7.52	57*	0.8	-	7.0E6	7.3E6	[4, 11, 37]
2-methylalanine, zwitterion	-0.60	6	0	-7.57	51*	0.6	-	1.1E8	1.2E7	[11, 37, 41]
water	n/a	2	0	-10.31	15.7*	1.0	-	1.3E5	2.4E5	[42]
propene**	-0.47	0	3	-6.97	43	0.3	0.8	7.0E9	3.8E9	[4]

$D_n(r)$, nucleophilic delocalizability (taken as maximum value on carbon in the parent molecule); σ, number of σ-type H-atoms; π, number of π -type H-atoms; E_{HOMO}, energy of the highest occupied molecular orbital (eV); pK_a, proton dissociation constant; c^2, squared atomic orbital coefficient; k_r(exp)/k_r(pred), experimental/predicted rate constant for reaction with OH$^{\bullet}$ (M^{-1}s^{-1}).

* Errors reflect the discrepancy between reported values.

** reacts with OH$^{\bullet}$ via hydrogen abstraction

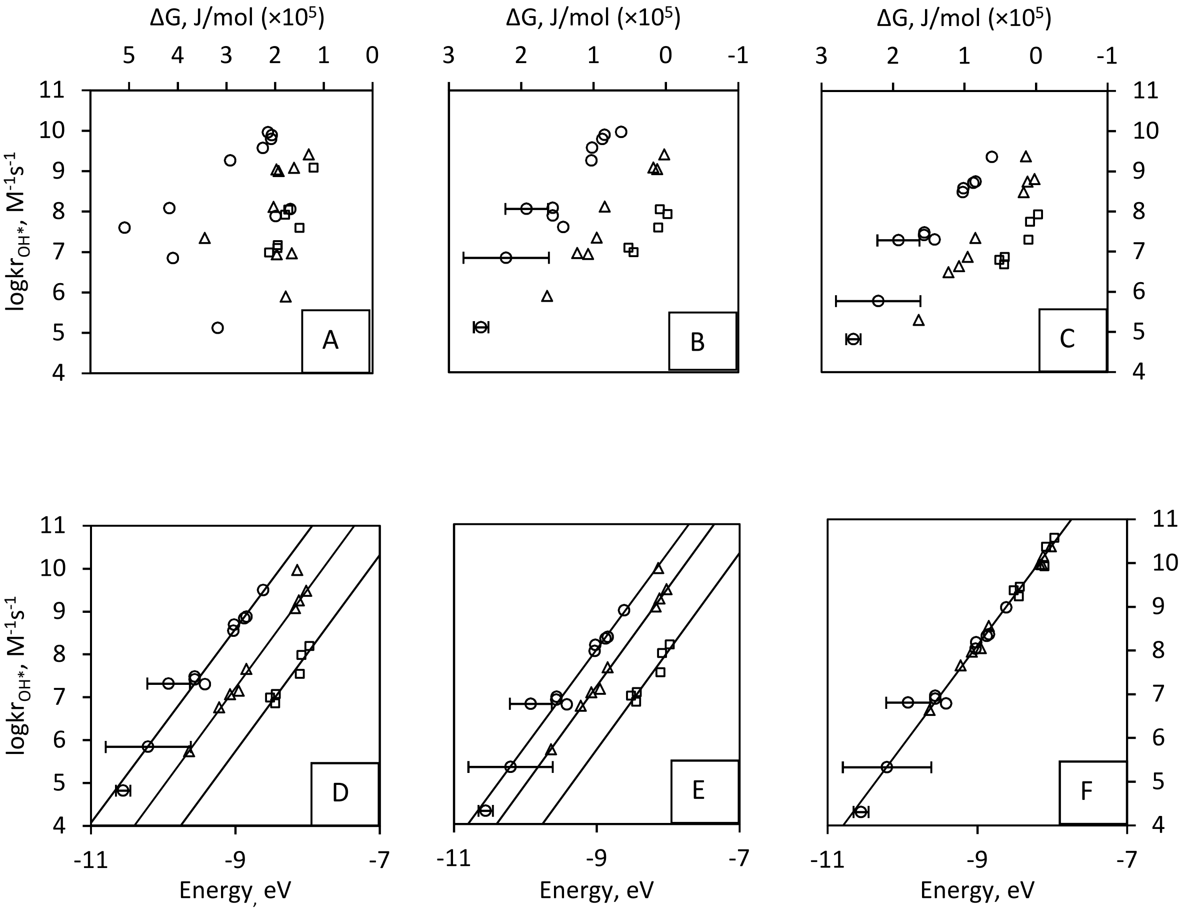

Figure S8. Rate constants (log k_r) for reaction with OH$^\bullet$ (y), versus reaction energies (x). Calculations performed using:

A: Equation 6 (y = E_{HOMO})

B: Equation 7

C. Equation 7 (k_r corrected for ∑(σ)+∑(π)

D. Equation 7 (k_r corrected for ∑(σ)+∑(π) and c_{HOMO}^2)

E. Equation 8, μ not included

F. Equation 8, μ included

Triangles and squares represent π-type X-H (polar, and zwitterionic, resp.) and circles represent σ-type X-H bonds. Solid lines denote data fits. Only symmetric compounds (with equivalent X-H groups) are taken into account. Energies in eV were converted to J/mol using 100 kJ/mol ≙ 1.04 eV and taking 0 kJ ≙ -8 eV ≈ E_{SOMO}(OH$^\bullet$). Corresponding data and computations in Table SI2. Error bars indicate uncertainty introduced upon prediction of pK_a (via the Chemaxon program [11]).

S4. Model evaluation

Eq. 8 was used to calculate partial and overall rate constants for molecules with different H atom types (results are given in Fig. S9-1 and Fig. S9-2). The calculated partial rate constants can differ significantly with respect to the total rate constants, e.g. $5{\cdot}10^{7} \leq k_{r,HA,i} \leq 6{\cdot}10^{8}$ $M^{-1}s^{-1}$ compared to $k_{r,HA} \approx 6{\cdot}10^{9}$ $M^{-1}s^{-1}$ for octane since there are 18 C-H bonds in C_8H_{18} (Fig. 8). The calculated partial rate constants $k_{r,HA,i}$ (octane, σ-type H´s) are also summed to obtain total reaction rate constants $k_{r,HA}$ and compared to experimental values and only minor discrepancies were observed. Fig. S9-1 illustrates the capability of Eq. 8 to predict selectivity for HA by $OH^{\bullet}$. The observed 'rate constant' consists of the sum of all the individual rate constants of the different reaction mechanisms – the mechanism with the highest reaction rate will dominate.

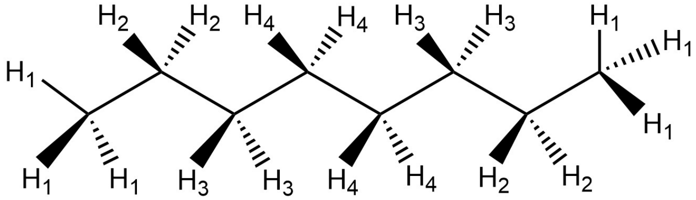

Atom type	H_1	H_2	H_3	H_4	Total
∑*i* (*i*=equivalent atom)	6	4	4	4	18
$k_{r,\,OH\bullet}$ ($M^{-1}s^{-1}$), Eq. 8	$5{\cdot}10^{7}$	$2{\cdot}10^{8}$	$4{\cdot}10^{8}$	$6{\cdot}10^{8}$	$6{\cdot}10^{9}$
$k_{r,\,OH\bullet}$ ($M^{-1}s^{-1}$), exp.	n/a	n/a	n/a	n/a	$\approx 1{\cdot}10^{10}$

Figure S9-1. Partial (*n*) and total reaction rate constants for $OH^{\bullet}$ (in $M^{-1}s^{-1}$, logarithmic) involving octane. Partial, i.e. site-specific hydrogen abstraction rates were calculated and summed to obtain the overall reaction rates using Equation 8.

Including *q*, Eq. 8 can describe symmetric molecules (Fig. S8, S11, S12), and was tested for non-symmetric molecules (Fig. S9-1 and Fig. S9-2). Selectivity is also evaluated for the benzylic hydrogen of 2'-deoxycytidine, $k_r = 10^{8}$ $M^{-1}s^{-1}$ (compared to $k_r = 10^{4}$ for a peripheral hydrogen) [43], the C–H hydrogen of methylamine, $k_r = 10^9$ (compared to $k_r = 10^7$ for N–H) [44], and the aldehydic hydrogen of pentanal, $k_r = 10^7$ (compared to $k_r = 10^5$ for the central β hydrogen) [45] (branching data from simulation or gas-phase studies [43-45]).

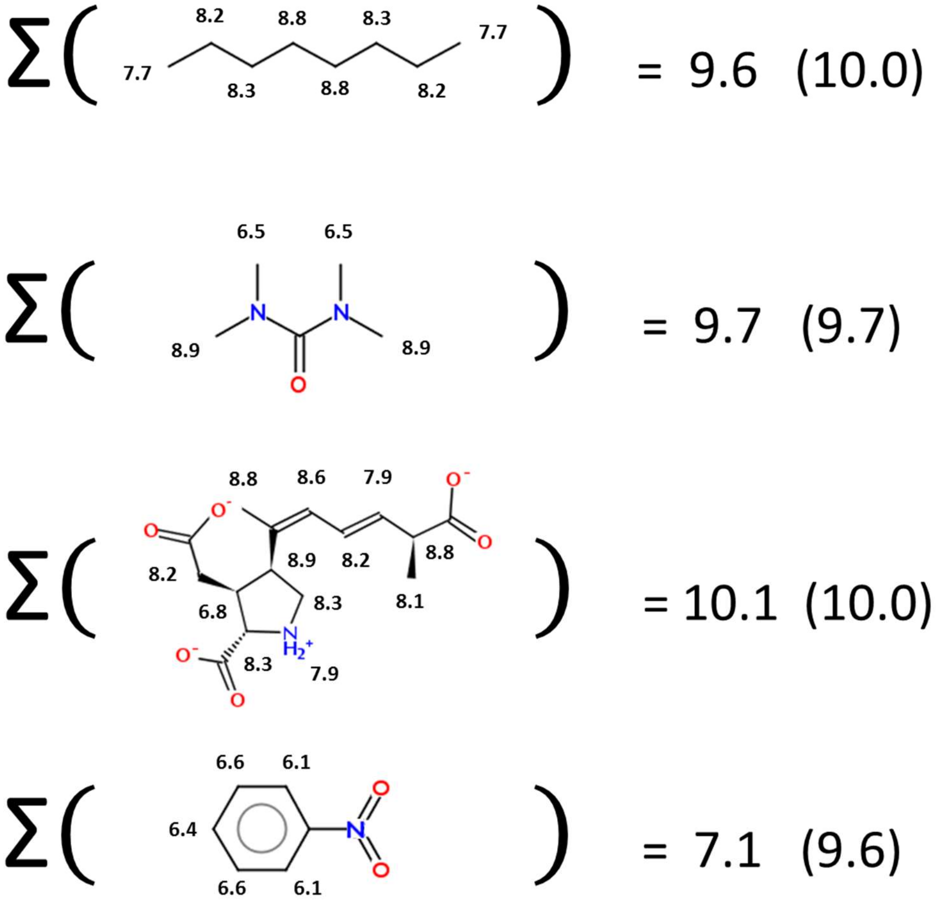

Figure S9-2. Partial and overall reaction rate constants for $OH^\bullet$ (in $M^{-1}s^{-1}$, logarithmic). Partial, i.e. site-specific hydrogen abstraction rates were calculated and summed to obtain the overall reaction rates using Equation 8. Values in parentheses denote experimentally obtained values.

The predicted values for octane (and 1,1,3,3-tetramethylurea and domoic acid) are intuitive: the partial charges on the different H atoms (Q_H) of octane, and by extension pK_a values, are similar (see Table. S2, [11]). Then, when only the level of substitution is relevant, tertiary R–H bonds react faster than secondary R–H bonds, which in turn react faster than primary R–H bonds (Fig. 8). Indeed, primary

C–H bonds are normally the strongest, and the BDE decreases for secondary and tertiary C–H bonds [46].

Electrophillic radicals often attack preferentially the most substituted, conjugated, and/or electron-rich position [47], which would be the weakest X–H bond (thermodynamic argument). Eq. 8 predicts higher rate constants for the more substituted and electron-rich sites, e.g. nitro-groups are meta-directing (Fig. S9-2). Fig. S9-1 and S9-2 illustrate that Eq. 8 can predict H atom abstraction selectivity for both σ-type (octane and methylamine [44]) and μ-type (2′-deoxycytidine [43], pentanal [45], domoic acid, nitrobenzene and tetramethylurea) H-donors by $OH^{\bullet}$.

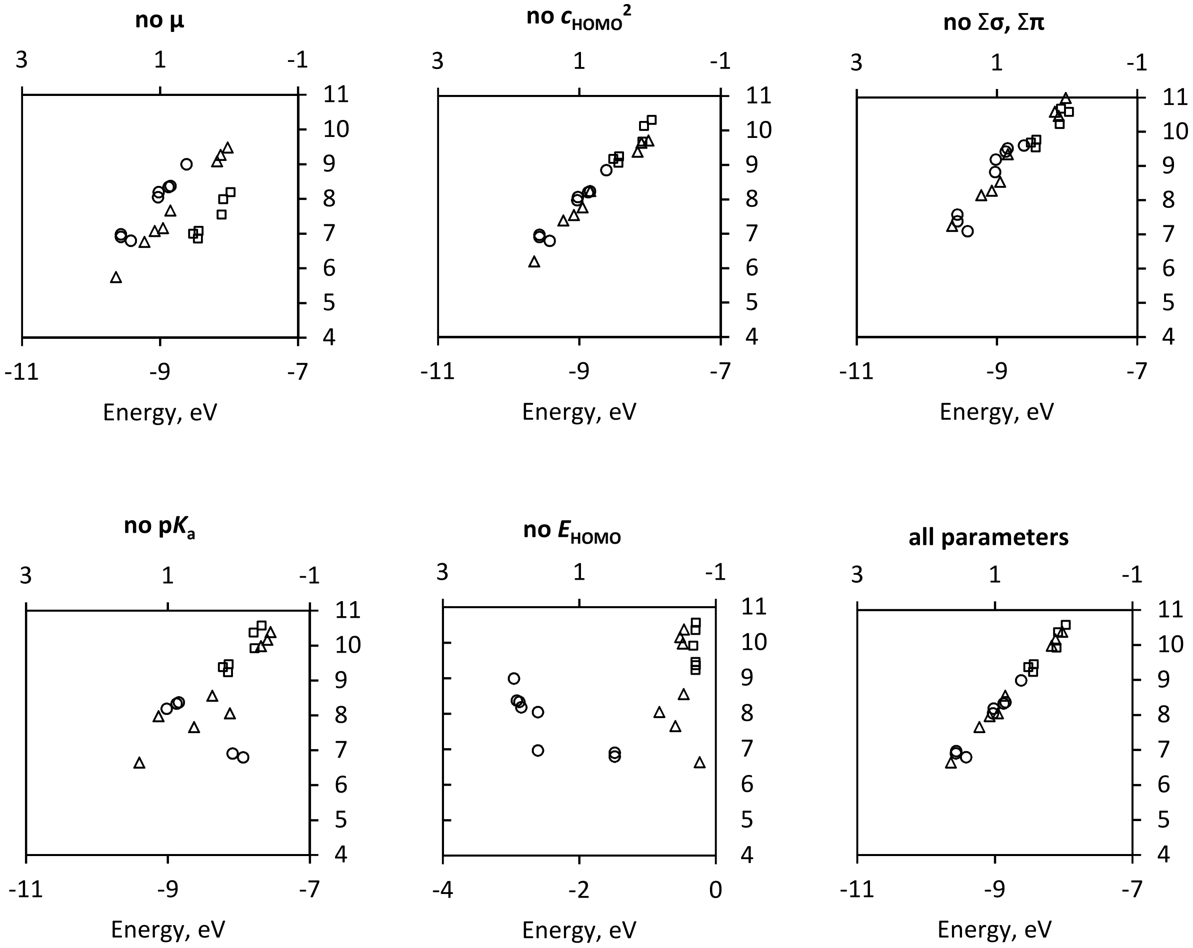

Figure S10. Parameter sensitivity analysis. The titles of the graphs indicate the parameter not included in the calculation. Compounds with error bars (Fig S8) and propene were excluded.

Table T3. Data used to predict k_r (H•) in Fig. S11. pK_a for alpha C-H of amino acid analogs were taken to be 16.5, see Stroud et al. (1983).

Compound name	$D_n(r)$	σ	π	E_{HOMO}	pK_a	c_{HOMO}^2	μ_π	k_r(exp)	Refs
Hexamethyleneimine, conjugate acid	-0.43	4	0	-6.25	55.1	0.85	-	1.4E7	[4, 11]
Water	n/a	2	0	-10.31	15.7	1.00	-	5.5E2	[4]
Trimethylamine	-0.49	9	0	-5.98	48±8*	0.73	-	2.0E8	[11, 36, 37]
Chloroform	n/a	1	0	-7.55	23±7*	0.69	-	1.1E7	[4, 11, 48]
Cyclopentane	-0.42	10	0	-5.88	60	0.87	-	8.5E7	[4, 11, 36, 37]
Trimethylammonium ion	-0.35	9	0	-7.58	39.4	0.93	-	2.0E6	[4, 11, 37]
2,6-Di-tert-butyl-4-methylphenol	n/a	1	0	-7.09	11.6	0.28	-	2.0E10	[4, 11]
Cyclohexane	-0.43	12	0	-5.74	60	0.86	-	7.5E7	[4, 11, 36, 37]
Tetrahydrofuran	-0.48	4	0	-6.50	44.0	0.77	-	7.2E7	[4, 11]
Cyclopropane	-0.40	6	0	-6.76	55	0.89	-	6.0E5	[4, 11, 36, 37]
Glycine, zwitterion	-0.60	0	2	-8.22	16.5	0.79	13.1	7.1E4	[4, 40]
Succinate ion	-0.60	0	4	-7.13	19.3	0.74	13.1	1.0E7	[4, 11]
Nitrilotriacetate ion	-0.60	0	6	-6.53	18.1	0.55	13.1	5.0E8	[4, 11]
Citrate ion	-0.60	0	4	-7.36	14.9	0.75	13.1	2.0E7	[4, 11]
propene**	-0.47	0	3	-6.97	43	0.25	0.8	5.3E9	[4]

* Errors reflect the discrepancy between reported values.

** Reacts with H• via addition

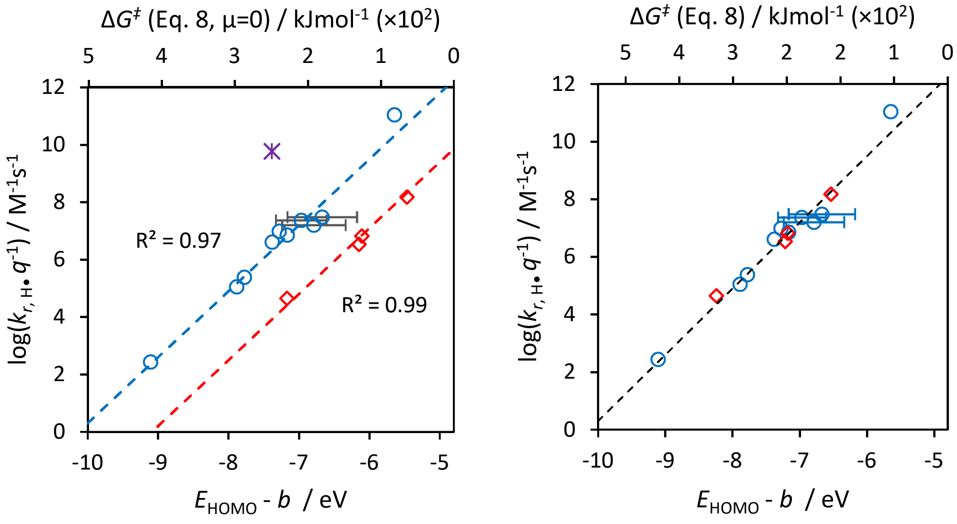

Figure S11. Rate constants for reaction with $H^{\bullet}$ (y), log k_r for $H^{\bullet}$. Energies were calculated using Eq. 8, (μ not included in A, μ included in B). Dashed lines denote the theoretical values based on Eq. 8. Squares are π-type zwitterionic R-H, triangles are π-type polar R-H and circles are σ-type R-H. Error bars indicate uncertainty introduced upon prediction of pK_a [11]. The star symbol denotes propene. Energies in eV were converted to J/mol using 100 kJ = 1.04 eV and taking 0 kJ ≙ -3.7 eV. For corresponding data see Table SI3.

Table T4. Data used to predict k_r ($CH_3^{\bullet}$) in Fig. S12. pK_a for alpha C-H of amino acid analogs were taken to be 16.5, see Stroud et al. (1983).

Compound name	$D_n(r)$	σ	π	E_{HOMO}	pK_a	c_{HOMO}^2	μ_π	k_r(exp)	Refs
acetonitrile	-0.53	0	3	-8.13	25	0.51	4.9	1.0E2	[4]
acetone	-0.59	0	6	-8.35	19.3	0.48	4.9	1.0E3	[4, 39]
glycine, negative ion	-0.62	0	2	-6.93	18.3	0.37	13.1	2.3E4	[11, 49]
methyl propionate	-0.60	0	2	-7.90	22	0.43	4.9	2.9E3	[4, 11]
3-pentanone	-0.60	0	4	-7.80	20.7	0.37	4.9	1.4E4	[4, 11]
2-methylpropionitrile	-0.54	0	1	-7.25	25.5	0.38	4.9	4.5E3	[4, 11]
D,L-alanine anhydride	-0.63	0	2	-7.36	19.6	0.25	4.9	1.2E5	[11, 50]
glycine anhydride	-0.64	0	4	-7.71	19.7	0.25	4.9	4.0E4	[11, 50]
sarcosine anhydride	-0.64	0	4	-7.57	19.4	0.21	4.9	4.0E4	[11, 50]
glycine, zwitterion	-0.60	0	2	-8.22	16.5	0.63	13.1	2.0E1*	[4, 40, 49]
propionitrile	-0.54	0	2	-7.66	30±3*	0.44	4.9	1.2E3	[4, 11, 51, 52]
hydrogen peroxide	n/a	2	0	-8.48	11.8	0.41	-	2.7E4	[4]
propene**	-0.47	0	3	-6.97	43	0.25	0.8	5.3E3	[4]

$D_e(r)$, electrophilic delocalizability; σ, number of σ-type H-atoms; *π*, number of π-type H-atoms; E_{HOMO}, energy of the highest occupied molecular orbital (eV); pK_a, proton dissociation constant; c^2, squared atomic orbital coefficient; k_r(exp)/k_r(pred), experimental/predicted rate constant for reaction with $CH_3^{\bullet}$ ($M^{-1}s^{-1}$).

* Errors reflect the discrepancy between reported values. Data from NIST database on alcohols [53] omitted, due to inconsistency with data from [54].

** Reacts with $CH_3^{\bullet}$ via addition

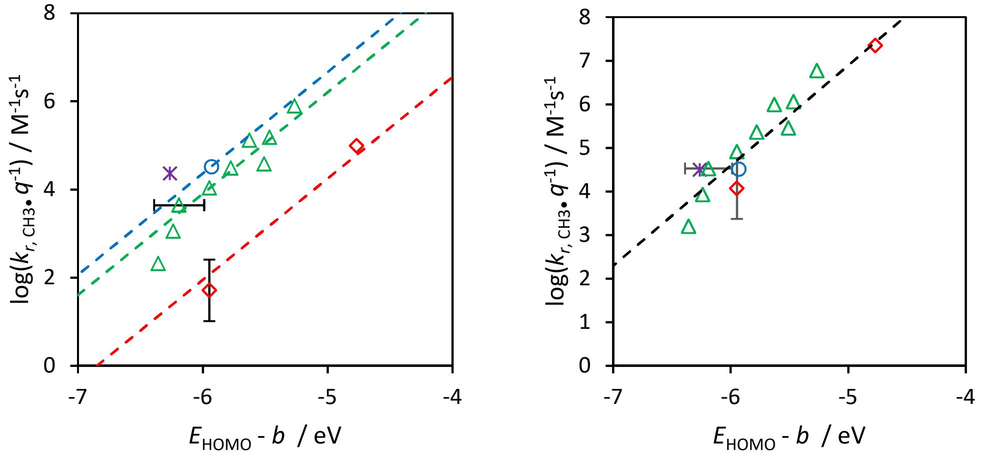

Figure S12. Rate constants for reaction with $CH_3^{\bullet}$ (y), log k_r for $CH_3^{\bullet}$· Energies were calculated using Eq. 8, (μ not included in A, μ included in B). Dashed lines denote the theoretical values based on Eq. 7. Red diamonds are π-type zwitterionic R-H, green triangles are π-type polar R-H and blue circle is σ-type R-H. Error bars indicate uncertainty, e.g. prediction of pK_a [11]. The star symbol denotes propene. Energies in eV were converted to J/mol using 100 kJ = 1.04 eV and taking 0 kJ ≙ -3.7 eV. For corresponding data see Table T4.

Table T5. Physico-chemical properties of the radicals considered, and their respective statistical reproducibility of Eq. 8.

radical/ conjugate H-donor	σ (p(k_r)/eV)	E_{SOMO}[a] (eV)	pK_a (X–H)	*BDE* (R–H) (kJ/mol)[b]	Enthalpy of formation (R·) ΔH_f^{0}[b], (kJ/mol)	R^2 Eq. 5	R^2 Eq. 6 (HA)	R^2 Eq. 8 (HA)
$OH^•$ / H_2O	2.2(±0.1) (ET) 2.3 (HA)	-8.0	11.5 [55]	499[d]	33.9[c]	0.93 (ET, N=36) 0.20 (HA, N≈500)	0.47-0.69 (N≈500)	0.98 (N=26)
$HOO^•$/ H_2O_2 [9]	2.1	-5.7	11.7	374[d]	13.4[c]	0.92	-	-
$CH_3^•$/ CH_4	2.6(±0.3)	-4.8	≈55	431[d]	144.0[c]	- 0.50 (HA, N=12)	0.61 (N=12)	0.93 (N=12)
$H^•$ /H_2	2.4(±0.1) 2.1(±0.1)	-4.0	22 ± 2 [56]	436[d]	-	- 0.40 (HA, N=14)	0.73 (N=12)	0.98 (N=14)
$O_2^{•-}$ [9]	2.5	-3.8	N/A	N/A	-	0.84	-	-

a: calculated using restricted open-shell Hartree Fock (ROHF) using the PM7 method, see the section on descriptor calculation (S2)

b: for the gas phase

c: [57]

d: [58]

S5. Radical electrophilicity

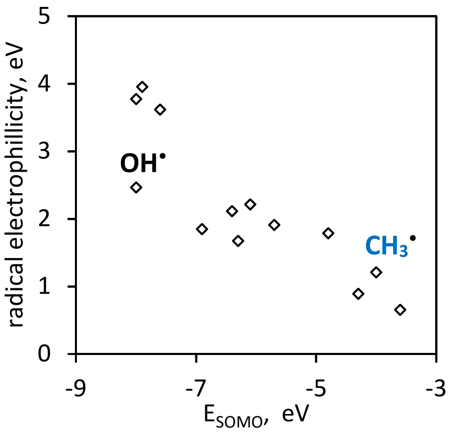

Figure S13: Radical electrophillicity [59] versus E_{SOMO}.

Table T6. Radical electrophilicities obtained by deVleeschouwer et al. [59] and E_{SOMO} values obtained in this study.

Radical	Electrohillicity (ω), eV [59]	E_{SOMO}, eV
tert-butyl	0.651	-3.6
methyl	1.209	-4.0
hydrogen	1.788	-4.8
hydroperoxyl	1.911*	-5.7
hydroxyl	2.462	-8.0
fluorine	3.954	-7.9
ethyl	0.891	-4.3
difluoroamino	1.849	-6.9
trifluoromethyl	1.672	-6.3
ethoxy	2.114	-6.4
ethylsulfide	2.214	-6.1
chlorine	3.772	-8.0
bromine	3.614	-7.6

* interpolated value

S6. Radical addition

Describing the kinetics for addition was beyond the scope of this investigation. Figure S13 indicates the influence of aromaticity on k_r. Aromaticity decreases $\Delta G^{\ddagger}$ because of bonding-like interactions and delocalization in the transition state (stabilization) resulting in higher rate constants compared to ET or even HA [2, 60], see also nitrobenzene in Fig. S9 and propene in Fig. S11 and S12. However, low $\Delta G^{\ddagger}$ might be counterbalanced by substantially negative activation entropy. Clearly, Eq. 8 would need to be adapted to allow predictions for aromatic moieties. Like for HA, addition is driven more by relative bond strengths than by FMO interaction alone. For HA a charge-transfer interaction was included to characterize ΔG_r (Eq. S1), and the same may be needed for addition. Diffusion is not considered in Eq. S1, and would need to be considered for addition as well, as well as branching [61].

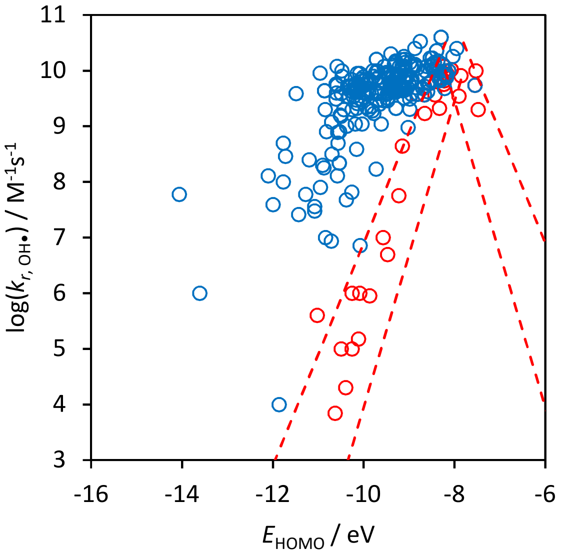

Fig. S14. The rate constant for reaction with $OH^{•}$ versus the energy of the highest occupied molecular orbital (E_{HOMO}). Red and blue circles denote electron transfer and addition, respectively.

S7. Discussion of associated uncertainties

Simulations are often carried out to avoid experimentation [62]. Ideally, to facilitate 'screening' of many chemicals in a short timeframe, simulations are mechanistically interpretable and computationally inexpensive [63]. The latter makes 'ab-initio' methods not desirable for the present purpose. While lowering the cost (time and money), simulations should remain within "acceptable" levels of uncertainty. Here, we evaluated the sensitivity of Eq. 8 to changes in its parameters. We discuss uncertainties in the light of these results (Fig. S10) and related studies.

Formulaic

Our study unifies 5 parameters (Fig. S8F) into a single reactivity parameter which generates robust semi-quantitative data with little computational effort and minimal complexity. The parameters are similar to those selected previously [21], and include E_{HOMO}, average net charges on H, surface area and μ. Wang et al. (2009) combined these via multiple linear regression (MLR). In contrast, we combined descriptors into Eq. 8 using formulae describing thermochemical principles. Thus, the prediction of $\Delta G^{‡}$ via Eq. 8 corresponds more to a physical model. This could explain the higher correlation in Fig. S8F ($R^2 = 0.98$) compared to e.g. $R^2 = 0.90$ and $Q_{\mathrm{LMO}}^2 = 0.81$ obtained using MLR [21] and illustrates that prediction uncertainty can arise from the use of a particular statistical method.

Eq. 8 does not consider diffusion. Steric hindrance increases the activation energy due to rearrangement (entropy term) [60, 61]. The steady-state Smoluchowski rate equation [64] and (solvent-) accessible surface area might be useful for site-specific corrections. Such corrections are straightforward if molecules are symmetric, i.e. when sites have equal probabilities to react [65]. Changes in entropy are similar for related reactions; if one can assume that $T\Delta S$ is some monotonic function of ΔH, predictions are easier [20]. The TS barrier might be circumvented entirely via tunneling, [42]. Considering the molecules in the current datasets (TS2-S4), Figs. S10B, S10C and previous results [16], we expect these influences small. The geometry of the abstraction pathway can be susceptible to change in partial charge via the angle of attack [66]. Also, the avoided crossing framework [67, 68] can describe more explicitly (additional) influences resulting from the charges of the reagents, excited states and intermediates [28, 69].

Transfer of the electron

$\Delta G^{\ddagger}$ is the most sensitive to changes of the parameter E_{HOMO}. (Fig. S10E). For uncertainties relating to QC calculations, we refer to [6, 7] and S2. Highly polarized unsaturated and inorganic molecules were generally outliers (Fig. S3). Electron withdrawing groups normally stabilize σ-bonds towards electrophilic attack, but instead show relatively high k_r. E_{LUMO}, atomic orbital coefficients, group- or atom-specific charges and delocalizability indices [65, 70] might help to explain k_r for such compounds. Charge transfer involving atoms other than the proton might be involved. For these reasons, haloacetates were disregarded in the current study. Electron affinity and E_{SOMO} (of the radical) are equally important [27].

E_{SOMO} is never a single value but rather represents a ratio of two spin states α-SOMO and β-SOMO, which can have different energies [71-74]. The calculation of electron affinity via semi-empirical methods is less accurate compared to ionization potential, potentially due to specific solvent effects [6, 9] such as lone pair–π interactions [75]. The E_{HOMO} and E_{SOMO} values are fairly high [4], potentially due to the semi-empirical nature of the method and specific solvent interactions [7]. For LFER consideration, absolute values have little physical meaning. Therefore, we only used differences in the calculations. The same applies to $OOH^{\bullet}$, $H^{\bullet}$ and $CH_3^{\bullet}$ (Table T5).

Transfer of the proton

The influence of pK_a on ΔG (Fig. 3B) and $\Delta G^{\ddagger}$ is substantial (Fig. S10D). Determination of partial charges and pK_a is not straightforward [76]. A portion of the scatter in the figures stems from inaccuracies in the term $2.3RT\text{p}K_{a(X\text{–}H)}$ as compared to E_{HOMO}, in case proton transfer dominates the reaction enthalpy. For example, $50 \leq \text{p}K_a \leq 60$ [11, 36, 37] (±0.6 eV) and $25 \leq \text{p}K_a \leq 34$ [11, 51, 52] (±0.5 eV) have been reported for methane and propionitrile, respectively (Table T4). The derivation of proton transfer energies via pK_a (using the program ChemAxon [11]) introduced uncertainty because partial charges on atoms other than H, as well as inductive [77] and thermodynamic [78] effects determine proton transfer energies (Tables T2-4, error bars in Fig. 6B, 6C, S8, S11 and S12). Solvation effects on ΔG are not included in equation Eq. 5 (and Eq. S1). Note that it is possible to infer the pK_a value from k_r and E_{HOMO}, similar to electrochemical methods for otherwise difficult to measure compounds [79, 80].

The protonation state (pK_a/pH) of the oxidant also affects the kinetics. $O^{\bullet-}$ is a less effective oxidant than $OH^{\bullet}$ and the lifetime of the water radical cation ($H_2O^{\bullet+}$) is short, <1 ps [81] (low pK_a). Thus, the observed k_r is likely to be proportional to the speciation of $OH^{\bullet}$ as a function of pH. For k_r ($OH^{\bullet}$) the mean experimental pH was 7 (pH>11 excluded, S1), implying that $OH^{\bullet}$ is in its neutral form (≥99.99%).

Matrix characteristics

LFERs relate $\Delta G^{\ddagger}$ to the thermodynamic equilibrium (relative strength of R–H and X–H). However, for ‘non-similar’ molecules $\Delta G^{\ddagger}$ is not necessarily proportional to ΔG_r and the ‘details’ of the mechanism ($\Delta G_{\text{TS}}^{\ddagger}$) cannot be ignored. The dipole moment characterized partially the effect of solvation, influencing $\Delta G_{\text{TS}}^{\ddagger}$ (Fig. 6) and $\Delta G^{\ddagger}$ (Fig. S10A). Statistical significances of correlations [33, 82] between QC parameters and k_r can be lower for aqueous-phase as compared to the gas phase due to 1) improper description of the dielectric continuum, or 2) specific QC and thermodynamic effects. Here, we assumed that the dielectric constant of the solvent is constant over the range of pH considered, while this is not necessarily the case. The effect of solvation on ΔG_r can be included via summation, but is expected to be minimal since hydrogen abstraction does not involve a net change in charge.

The influence of solvation and the presence of counterions on the energy levels of the molecules [83], can be described more accurately by using hybrid QM/MM or microsolvation methods [82, 84] but still involve uncertainties for large, complex and heterogeneous molecules while 'ab-initio' calculations are not practical for screening. The sensitivity of $\Delta G_{TS}^{\ddagger}$ on the dipole moment (Fig. S10A) is connected to delocalizability (via Eq. 8). Indeed, finer details of the energy-reaction coordinate can be determined by charge redistribution [85].

Other matrix effects, reaction/complexation with impurities, buffering or chelating agents and ionic strength impacts may play a role [9, 86]. The influence of temperature also should be considered explicitly [83]. The error introduced by combining different experimental conditions and methods might explain the residual variances in Fig. 7C, Fig. S10 and S12, though they are small. For speciation mixtures, the Henderrson-Hasselbalch equation applies [87, 88]. The calculation of QC descriptors uses explicit protonation states. Therefore, the parameters in Eq. 8 may characterize some experimental uncertainty.

REFERENCES

1. Luo, X., et al., *Development of a QSAR model for predicting aqueous reaction rate constants of organic chemicals with hydroxyl radicals.* Environmental Science-Processes & Impacts, 2017. **19**(3): p. 350-356.
2. Buxton, G.V.G., C.L.; Helman, W.P.; Ross, A.B., *Critical Review of Rate Constants for Reactions of Hydrated Electrons, Hydrogen Atoms and Hydroxyl Radicals (.OH/.O-) in Aqueous Solution.* J. Phys. Chem. Ref. Data, 1988. **17**: p. 513.
3. L.M. Dorfman, G.E.A., *Reactivity of the Hydroxyl Radical in Aqueous Solutions*. 1973: US Department of Commerce. National Bureau of Standards.
4. NIST. *NDRL/NIST solution kinetics database on the web*. 2002.
5. O'Boyle, N.M., et al., *Open Babel: An open chemical toolbox.* Journal of Cheminformatics, 2011. **3**.
6. Stewart, J.J.P., *MOPAC*. 2016, Stewart Computational Chemistry: Colorado Springs, CO, USA.
7. Stewart, J.J.P., *Optimization of parameters for semiempirical methods VI: more modifications to the NDDO approximations and re-optimization of parameters.* Journal of Molecular Modeling, 2013. **19**(1): p. 1-32.
8. Nolte, T.M. and W.J.G.M. Peijnenburg, *Aqueous-phase photooxygenation of enes, amines, sulfides and polycyclic aromatics by singlet (a1Δg) oxygen: prediction of rate constants using orbital energies, substituent factors and quantitative structure–property relationships.* Environmental Chemistry, 2018. **14**(7): p. 442-450.
9. T.M. Nolte, W.J.G.M.P., *Aqueous-phase reaction between organic chemicals and superoxide/hydroperoxyl radicals (HO2·/O2·-) – Relationships between oxidation and reduction rate constants and quantum-chemical descriptors.* Free Radical Research, 2018. **accepted**.
10. Wishart, D.S., et al., *DrugBank: a knowledgebase for drugs, drug actions and drug targets.* Nucleic Acids Research, 2008. **36**: p. D901-D906.
11. ChemAxon, *Calculator Plugin for structure property prediction. MarVin Version 5.2.0*.
12. Manchester, J., et al., *Evaluation of pKa estimation methods on 211 druglike compounds.* J Chem Inf Model, 2010. **50**(4): p. 565-71.
13. Nicklaus, C.L.M.C., *Comparison of Nine Programs Predicting pKa Values of Pharmaceutical Substances.* J. Chem. Inf. Model., 2009. **49**: p. 2801–2812.
14. Tauber, J., D. Imbri, and T. Opatz, *Radical addition to iminium ions and cationic heterocycles.* Molecules, 2014. **19**(10): p. 16190-16222.
15. KiecKononowicz, K., J. KarolakWojciechowska, and J. Robak, *Fused 2-thiohydantoin derivatives: Evaluation as potential antioxidants.* Archiv Der Pharmazie, 1997. **330**(4): p. 85-90.
16. Minakata, D., *DEVELOPMENT OF AQUEOUS PHASE HYDROXYL RADICAL REACTION RATE CONSTANTS PREDICTORS FOR ADVANCED OXIDATION PROCESSES*. 2010, Georgia Institute of Technology.
17. Szreder, T.B., K,; Bojanowska-Czajka, A.; Kisala, J.; Pogocki, D.; Trojanowicz, M., *Investigation of decomposition mechanism of perfluorooctanoate anion (PFOA) in water by ionizing radiation*, in *Pulse* 2018, poster presentation: Lodz, Poland.
18. Lewis, E.S., *Sn2 and Single-Electron-Transfer Mechanisms - the Distinction and Relationship.* Journal of the American Chemical Society, 1989. **111**(19): p. 7576-7578.
19. Rosta, E. and A. Warshel, *On the Origins of the Linear Free Energy Relationships: Exploring the Nature of the Off-Diagonal Coupling Elements in S(N)2 Reactions.* J Chem Theory Comput, 2012. **8**(10): p. 3574-3585.
20. Jensen, W.B., *Lewis Acid-Base Definitions - Status-Report.* Chemical Reviews, 1978. **78**(1): p. 1-22.

21. Wang, Y.N., et al., *Estimation of Aqueous-Phase Reaction Rate Constants of Hydroxyl Radical with Phenols, Alkanes and Alcohols.* Qsar & Combinatorial Science, 2009. **28**(11-12): p. 1309-1316.
22. Bartolotti, L.J. and E.O. Edney, *Investigation of the Correlation between the Energy of the Highest Occupied Molecular-Orbital (Homo) and the Logarithm of the Oh Rate-Constant of Hydrofluorocarbons and Hydrofluoroethers.* International Journal of Chemical Kinetics, 1994. **26**(9): p. 913-920.
23. Moores, L.C., *Hydroxyl radical additions to arenes*. 2015, Ball State University: Muncie, Indiana. p. 99.
24. Zhuo, L.G., W. Liao, and Z.X. Yu, *A Frontier Molecular Orbital Theory Approach to Understanding the Mayr Equation and to Quantifying Nucleophilicity and Electrophilicity by Using HOMO and LUMO Energies.* Asian Journal of Organic Chemistry, 2012. **1**(4): p. 336-345.
25. Bordwell, F.G., et al., *Bond-Dissociation Energies in Dmso Related to the Gas-Phase.* Journal of the American Chemical Society, 1991. **113**(26): p. 9790-9795.
26. Babkin, V.A.F., R.G.; Minsker, K.S.; Ponoparev, O.A.; Sangalov, Y.A.; Berlin, A.A.; Zaikov, G.E., *Connection of the universal acidity index of H-acids with the charge on hydrogen atom (ab initio method).* Oxidation communication, 2002. **25**(1): p. 21-47.
27. Klopman, G., *Chemical-reactivity and the concept of charge-controlled and frontier-controlled reactions.* Current Contents/Engineering Technology & Applied Sciences, 1984(20): p. 16-16.
28. Fukuzumi, S. and J.K. Kochi, *Electrophilic Aromatic-Substitution - Charge-Transfer Excited-States and the Nature of the Activated Complex.* Journal of the American Chemical Society, 1981. **103**(24): p. 7240-7252.
29. Pirovano, A., et al., *Mechanistically-based QSARs to Describe Metabolic Constants in Mammals.* Atla-Alternatives to Laboratory Animals, 2014. **42**(1): p. 59-69.
30. Lewis, D.F.V., *Frontier orbitals in chemical and biological activity: Quantitative relationships and mechanistic implications.* Drug Metabolism Reviews, 1999. **31**(3): p. 755-816.
31. Kandasamy, S. and K. Rathinam, *A comparative DFT study on the antioxidant activity of apigenin and scutellarein flavonoid compounds.* Molecular Physics, 2011. **109**(6): p. 839-852.
32. Sun, Y.J., et al., *Quantitative Structure-activity Relationship Studies on the Antioxidant Activity and Gap Junctional Communication of Carotenoids.* Chinese Journal of Structural Chemistry, 2010. **29**(9): p. 1362-1372.
33. Gligorovski, S., et al., *Rate Constants for the OH Reactions with Oxygenated Organic Compounds in Aqueous Solution.* International Journal of Chemical Kinetics, 2009. **41**(5): p. 309-326.
34. DeMore, W.B. and K.D. Bayes, *Rate constants for the reactions of hydroxyl radical with several alkanes, cycloalkanes, and dimethyl ether.* Journal of Physical Chemistry A, 1999. **103**(15): p. 2649-2654.
35. Pompe, M., et al., *Using variable and fixed topological indices for the prediction of reaction rate constants of volatile unsaturated hydrocarbons with OH radicals.* Molecules, 2004. **9**(12): p. 1160-1176.
36. Smith, M.B.M., J., *March's Advanced Organic Chemistry. Reactions, Mechanisms and Structure*. 6 ed. 2007: Wiley.
37. McMurry, J.E., *Chapter 9. Alkynes: An Introduction to Organic Synthesis*, in *Organic Chemistry*, L. Lockwood, Editor. 2010, Brooks/Cole. p. 326.
38. Parker, G.K.H., G.A. , *A Spectroelectrochemical Investigation of the Interaction of Gold with CyanoContaining Ligands.* ECS Transactions, , 2010. **28**(6): p. 223-235.
39. Keeffe, J.R.K., A.J., *In The Chemistry of Enols; Rappoport, Z.*, J.W.a. Sons, Editor. 1990: Chichester. p. 399−480.

40. Stroud, E.D., D.J. Fife, and G.G. Smith, *A Method for the Determination of the Pka of the Alpha-Hydrogen in Amino-Acids Using Racemization and Exchange Studies.* Journal of Organic Chemistry, 1983. **48**(26): p. 5368-5369.
41. Stefanic, I., et al., *Absolute rate constants and yields of transients from hydroxyl radical and H atom attack on glycine and methyl-substituted glycine anions.* Journal of Physical Chemistry A, 2001. **105**(38): p. 8681-8690.
42. Hand, M.R., et al., *Theoretical estimation of the activation energy for the reaction HO center dot+H2O -> H2O+center dot OH: Importance of tunneling.* Journal of Physical Chemistry A, 1998. **102**(29): p. 5958-5966.
43. W. Yao, X.M., S. Li, Y. Gao, F. Nian, L. Zhou, *Theoretical study of mechanism and kinetics for the reaction of hydroxyl radical with 2'-deoxycytidine.* Structural Chemistry, 2018.
44. Onel, L., et al., *Branching Ratios in Reactions of OH Radicals with Methylamine, Dimethylamine, and Ethylamine.* Environmental Science & Technology, 2014. **48**(16): p. 9935-9942.
45. Castaneda, R., et al., *Rate Constants and Branching Ratios in the Oxidation of Aliphatic Aldehydes by OH Radicals under Atmospheric Conditions.* Journal of the Mexican Chemical Society, 2012. **56**(3): p. 316-324.
46. Lide, D.R., *Handbook of Chemistry and Physics*. 80th Edition ed. 1999, Boca Raton, FL: CRC Press.
47. Davies, M.J., *Protein oxidation and peroxidation.* Biochemical Journal, 2016. **473**: p. 805-825.
48. Michigan State University, D.o.C. *Acidity tables for heteroatom organic acids and carbon acids*. 2019]; Available from: https://www2.chemistry.msu.edu/faculty/reusch/virttxtjml/acidity2.htm#carbacid.
49. Yardeni, G., et al., *H/D kinetic isotope effect as a tool to elucidate the reaction mechanism of methyl radicals with glycine in aqueous solutions.* J Phys Chem A, 2013. **117**(51): p. 13996-8.
50. Reid, D.L., et al., *H-Atom abstraction by C-centered radicals from cyclic and acyclic dipeptides. A theoretical and experimental study of reaction rates.* Physical Chemistry Chemical Physics, 2003. **5**(15): p. 3278-3288.
51. Riddick, J.A., W.B. Bunger, Sakano T.K., *Techniques of Chemistry* in *Organic Solvents*. 1985, John Wiley and Sons.: New York, NY. p. 584.
52. Dörwald, F.Z., *The Alkylation of Carbanions*, in *Side Reactions in Organic Synthesis: A Guide to Successful Synthesis Design*. 2005, Wiley-VCH: Weinheim. p. 145.
53. Thomas, J.K., *Pulse Radiolysis of Aqueous Solutions of Methyl Iodide and Methyl Bromide . Reactions of Iodine Atoms and Methyl Radicals in Water.* Journal of Physical Chemistry, 1967. **71**(6): p. 1919-&.
54. Gray, P. and A.A. Herod, *Methyl Radical Reactions with Isopropanol and Methanol Their Ethers and Their Deuterated Derivatives.* Transactions of the Faraday Society, 1968. **64**(550p): p. 2723-&.
55. Poskrebyshev, G.A., P. Neta, and R.E. Huie, *Temperature dependence of the acid dissociation constant of the hydroxyl radical.* Journal of Physical Chemistry A, 2002. **106**(47): p. 11488-11491.
56. Kelly, C.A. and D.R. Rosseinsky, *Estimates of hydride ion stability in condensed systems: energy of formation and solvation in aqueous and polar-organic solvents.* Physical Chemistry Chemical Physics, 2001. **3**(11): p. 2086-2090.
57. Janoschek, R. and M.J. Rossi, *Thermochemical properties of free radicals from G3MP2B3 calculations.* International Journal of Chemical Kinetics, 2002. **34**(9): p. 550-560.
58. Darwent, B.d., *Bond Dissociation Energies in Simple Molecules*. 1970, Washington, DC: US Department of Commerce National Bureau of Standards (NSRDS).
59. De Vleeschouwer, F., et al., *Electrophilicity and nucleophilicity index for radicals.* Organic Letters, 2007. **9**(14): p. 2721-2724.

60. Lexa, D., et al., *Single Electron-Transfer and Nucleophilic-Substitution - Reaction of Alkyl Bromides with Aromatic Anion Radicals and Low Oxidation-State Iron Porphyrins.* Journal of the American Chemical Society, 1988. **110**(23): p. 7617-7625.
61. Fang, X.W., H.P. Schuchmann, and C. von Sonntag, *The reaction of the OH radical with pentafluoro-, pentachloro-, pentabromo- and 2,4,6-triiodophenol in water: electron transfer vs. addition to the ring.* Journal of the Chemical Society-Perkin Transactions 2, 2000(7): p. 1391-1398.
62. Blanksby, S.J. and G.B. Ellison, *Bond dissociation energies of organic molecules.* Accounts of Chemical Research, 2003. **36**(4): p. 255-263.
63. ECHA, *Practical guide How to use and report (Q)SARs*. 2016.
64. Galano, A. and J.R. Alvarez-Idaboy, *Glutathione: mechanism and kinetics of its non-enzymatic defense action against free radicals.* Rsc Advances, 2011. **1**(9): p. 1763-1771.
65. Rorije, E., et al., *Modeling reductive dehalogenation with quantum chemically derived descriptors.* SAR QSAR Environ Res, 1995. **4**(4): p. 237-52.
66. Kovacevic, G. and A. Sabljic, *Atmospheric oxidation of halogenated aromatics: comparative analysis of reaction mechanisms and reaction kinetics.* Environmental Science-Processes & Impacts, 2017. **19**(3): p. 357-369.
67. Matzjasyewski K, D.T.P., *Chapter 1. Theory of radical reactions*, in *Handbook of radcial polymerization*. 2002, Wiley-Interscience: Hoboken.
68. Braun-Sand S., O.M.H.M., Warshell A., *Proton transport in carbonic anhydrase as an example of the difference between microscopic and phenomenological LFERs. In: Computer modelling of enzyme catalysis and its relationship to concepts in physical organic chemistry.*, in *Advances in Physical Organic Chemistry*, J.P. Richard, Editor. 2005, Elsevier: Amsterdam. p. 212-217.
69. Shaik, S.S., *The Lego Way - Curve Crossing Diagrams as General-Models in Physical Organic-Chemistry.* Pure and Applied Chemistry, 1991. **63**(2): p. 195-204.
70. Baumgartner, M.T., et al., *Theoretical study of the relative reactivity of chloroethenes with atmospheric oxidants (OH, NO3, O(P-3), Cl(P-2) and Br(P-2)).* Physical Chemistry Chemical Physics, 2002. **4**(6): p. 1028-1032.
71. Minakata, D., et al., *Experimental and theoretical studies on aqueous-phase reactivity of hydroxyl radicals with multiple carboxylated and hydroxylated benzene compounds.* Physical Chemistry Chemical Physics, 2015. **17**(17): p. 11796-11812.
72. Krenske, E.H. and C.H. Schiesser, *A comparison of orbital interactions in the additions of phosphonyl and acyl radicals to double bonds.* Organic & Biomolecular Chemistry, 2008. **6**(5): p. 854-859.
73. Sharp, E.N., P. Rupper, and T.A. Miller, *The structure and spectra of organic peroxy radicals.* Physical Chemistry Chemical Physics, 2008. **10**(27): p. 3955-3981.
74. A. Bottoni, J.F., D. Lefort *On the Role of the Orbital Interaction Concept in the Interpretation of Organic Free Radical Structures and Reactivities* in *Molecules in Physics, Chemistry and Biology* J. Maruani, Editor. 1989, Kluwer Academic Publishers Dordrecht. p. 173-219.
75. Scheiner, S., T. Kar, and J. Pattanayak, *Comparison of various types of hydrogen bonds involving aromatic amino acids.* Journal of the American Chemical Society, 2002. **124**(44): p. 13257-13264.
76. Alongi, K.S. and G.C. Shields, *Theoretical Calculations of Acid Dissociation Constants: A Review Article.* Annual Reports in Computational Chemistry, Vol 6, 2010. **6**: p. 113-138.
77. Varekova, R.S., et al., *Predicting pK(a) values from EEM atomic charges.* Journal of Cheminformatics, 2013. **5**.
78. Meloun, M. and Z. Ferencikova, *Enthalpy-entropy compensation for some drugs dissociation in aqueous solutions.* Fluid Phase Equilibria, 2012. **328**: p. 31-41.

79. R. Breslow, R.G., *An Electrochemical Determination of the pKa of Isobutane* J. Am. Chem. Soc., 1976. **98**(19): p. 6076–6077.
80. Nicholas, A.M.D. and D.R. Arnold, *Thermochemical Parameters for Organic Radicals and Radical Ions .1. The Estimation of the Pka of Radical Cations Based on Thermochemical Calculations.* Canadian Journal of Chemistry-Revue Canadienne De Chimie, 1982. **60**(17): p. 2165-2179.
81. Ma, J., F.R. Wang, and M. Mostafavi, *Ultrafast Chemistry of Water Radical Cation, H2O center dot+, in Aqueous Solutions.* Molecules, 2018. **23**(2).
82. Mitroka, S., et al., *How Solvent Modulates Hydroxyl Radical Reactivity in Hydrogen Atom Abstractions.* Journal of the American Chemical Society, 2010. **132**(9): p. 2907-2913.
83. Bjerrum, N., *Theory of the chemical reaction speed.* Zeitschrift Fur Physikalische Chemie--Stochiometrie Und Verwandtschaftslehre, 1924. **108**(1/2): p. 82-100.
84. M. Michalík; A. Vagánek, P.P., *Water effect on the bond dissociation energy of O–H and N–H bonds in phenol and aniline: The testing of simple molecular dynamics model.* Acta Chimica Slovaca, 2014. **7**(2).
85. Turro, N.J., *Chapter 7: Theoretical organic photochemistry, section 7.5*, in *Modern Molecular Photochemistry*. 1991, University Science Books: US. p. 207.
86. Truscott, T.G., *Pulse radiolysis and flash photolysis*, in *Photobiology*, R. E., Editor. 1991, Springer: Boston, MA.
87. Strong, B.F., *Synthesis of 1,1-Dialkyhydrazines and their Hydroxyl Radical Degradation in Aqueous Environments*. 2012, Western Michigan University.
88. Nolte, T.M. and A.M.J. Ragas, *A review of quantitative structure-property relationships for the fate of ionizable organic chemicals in water matrices and identification of knowledge gaps.* Environmental Science-Processes & Impacts, 2017. **19**(3): p. 221-246.